Fast and Simple Evaluation of the Catalysis and Selectivity Induced by External Electric Fields

Pau Besalú-Sala, Miquel Solà, Josep M. Luis,* and Miquel Torrent-Sucarrat*

ABSTRACT: In the oriented external electric-field-driven catalysis, the reaction rates and the selectivity of chemical reactions can be tuned at will. The activation barriers of chemical reactions within external electric fields of several strengths and directions can be computationally modeled. However, the calculation of all of the required field-dependent transition states and reactants is computationally demanding, especially for large systems. Herein, we present a method based on the Taylor expansion of the field-dependent energy of the reactants and transition states in terms of their field-free dipole moments and electrical (hyper)polarizabilities. This approach, called field-dependent energy barrier (FDB_β), allows systematic one-dimensional (1D), two-dimensional (2D), and three-dimensional (3D) representations of the activation energy barriers for any strength and direction of the external electric field. The calculation of the field-dependent FDB_β energy barriers has a computational cost several orders of magnitude lower than the explicit electric field optimizations, and the errors of the FDB_β barriers are within the range of only 1−2 kcal·mol^{-1}. The achieved accuracy is sufficient for a fast-screening tool to study and predict potential electric-field-induced catalysis, regioselectivity, and stereoselectivity. As illustrative examples, four cycloadditions (1,3-dipolar and Diels−Alder) are studied.

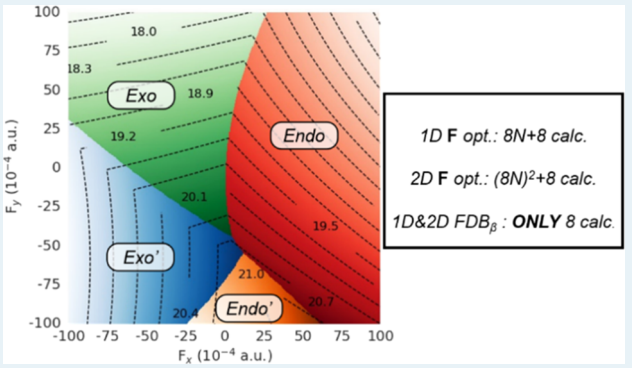

KEYWORDS: *reactivity, external electric field catalysis, cycloadditions, density functional calculations, regioselectivity, stereoselectivity*

INTRODUCTION

The interaction between molecules and external electric fields (EEFs) generates a broad range of effects.[1] Common observed phenomena are the changes in molecular geometry, vibrational structure, Stark effect, spin polarization, triggered electron transfer, chirality, and modification of absorption and emission properties.[2] Among them, the interest of the EEF effects on reactivity and selectivity is growing hugely since several practical applications of EEF-aided control on reactivity are being developed.[3] Since the field-induced change on regioselectivity in Diels−Alder (DA) reactions predicted by Shaik and co-workers[4] was experimentally validated,[3d] this chemistry is becoming more tangible and there has been a reborn of the topic also from the theoretical perspective.[5] Additionally, examples of the application of EEF on very diverse topics as the tuning of photo- and excited-state chemistry,[6] switch molecular diodes,[7] quantum tunneling,[8] and homo- and heterogeneous catalysis have been successfully investigated.[7,9]

One of the basic principles ruling the EEF potential applications is the control over the alignment between the molecule and the applied EEF. Currently, this new chemistry framework is investigated with the aid of very specific equipment as scanning tunneling microscopes,[10] and using laser-induced oscillating fields,[11] plasmonic modes in nanocavities,[12] and tribo- or piezoelectricity.[13] Therefore, improvements toward this direction are advancing by leaps and bounds.

The electric-field-induced chemistry can also be studied in the electrochemical double layer,[14] the interface layer between the electrode and the electrolyte. In this region, the molecular electron density of the reactants and their reactivity can be altered by the electric fields generated by the electrode.[15] The characterization of the electric field generated in the electrochemical double layer is a complex task, although the combination of the vibrational stark shift spectroscopy[16] and computational modeling is paving the way.[2a,17]

From another perspective, nature has been using electric fields to tailor its reactivity ubiquitously. Since the shape of the binding pockets of enzymes presents a well-defined structure of polar and charged amino acids, a local electric field (LEF) is

generated in the active site of enzymes.[18] The LEFs can, thus, promote electrostatic-induced catalysis in enzymes. Several works have already been reported, mainly focused on heme and nonheme iron proteins,[19] illustrating the LEFs potential utility in the control of reactivity and, more interestingly, selectivity.

Head-Gordon and co-workers[5e,20] and Hammes-Schiffer and co-workers[21] have used a bond dipole and electric field theoretical model to project the field onto the relevant bonds that are broken and formed along the reaction pathway. The difference between native and modified protein scaffolds allows the suggestion of possible mutations that tune the LEF to improve the enzyme efficiency.[22] For instance, this computational directed evolution has allowed an artificial Kemp Eliminase with a 43-fold improvement in the reaction rate of the enzyme.[23]

The main challenge of the computational evaluation of EEF effects on reactivity is the high amount of computational time requested since the number of calculations grows arithmetically with the number of electric-field strengths and directions investigated.[24] In this regard, the development of new computational methods is required to predict the reactivity and selectivity induced by EEFs at a feasible computational cost even when large chemical systems are involved. In this work, we present a new methodology to efficiently screen the effect on the reactivity and selectivity of an EEF applied with any strength and direction that can be used as a fast semiquantitative tool for the modeling, designing, and understanding of EEF-aided chemistry.

THEORY

The in-depth study of the field-dependent energy barriers (FDB) for one specific reaction involves computation of the reactants and the corresponding transition states (TSs) within external electric fields of several different strengths and directions. Consequently, it requires a tedious task that involves huge quantities of central processing unit (CPU) time even for medium-sized molecular systems.

For a given chemical system, the exact energy in the presence of an electric field can be expressed as a Taylor expansion around free-field energy

$$E^{\ddagger}(\mathbf{F}) = E^{\ddagger}(0) - \boldsymbol{\mu}\mathbf{F} - \frac{1}{2}\boldsymbol{\alpha}\mathbf{F}^2 - \frac{1}{6}\boldsymbol{\beta}\mathbf{F}^3 - \frac{1}{24}\boldsymbol{\gamma}\mathbf{F}^4 + \cdots \tag{1}$$

where $\mathbf{F}$ is the external electric field strength vector and $\boldsymbol{\mu}$, $\boldsymbol{\alpha}$, $\boldsymbol{\beta}$, and $\boldsymbol{\gamma}$ are the permanent dipole moment, the electrical polarizability matrix, and the first and second electrical hyperpolarizability tensors, respectively, defined as

$$\mu_i = -\left.\frac{\partial E}{\partial F_i}\right|_{F=0}; \quad \alpha_{ij} = -\left.\frac{\partial^2 E}{\partial F_i \partial F_j}\right|_{F=0}$$

$$\beta_{ijk} = -\left.\frac{\partial^3 E}{\partial F_i \partial F_j \partial F_k}\right|_{F=0}; \quad \gamma_{ijkl} = -\left.\frac{\partial^4 E}{\partial F_i \partial F_j \partial F_k \partial F_l}\right|_{F=0} \tag{2}$$

where the indices i, j, k, and l indicate Cartesian axes x, y, or z. Using eq 2 to express the field-dependent energy of the reactants and TS, the field-dependent energy barrier (FDB) of a reaction, $\Delta E^{\ddagger}(\mathbf{F})$, is given by

$$\Delta E^{\ddagger}(\mathbf{F}) = \Delta E^{\ddagger}(0) - \Delta\boldsymbol{\mu}^{\ddagger}\mathbf{F} - \frac{1}{2}\Delta\boldsymbol{\alpha}^{\ddagger}\mathbf{F}^2 - \frac{1}{6}\Delta\boldsymbol{\beta}^{\ddagger}\mathbf{F}^3 - \frac{1}{24}\Delta\boldsymbol{\gamma}^{\ddagger}\mathbf{F}^4 + \cdots \tag{3a}$$

$$\Delta E^{\ddagger} = (E_{TS} - E_R); \quad \Delta\mathbf{P}^{\ddagger} = (\mathbf{P}_{TS} - \mathbf{P}_R) \tag{3b}$$

where $\mathbf{P} = \boldsymbol{\mu}$, $\boldsymbol{\alpha}$, $\boldsymbol{\beta}$, and $\boldsymbol{\gamma}$, and $E_{TS}(\mathbf{P}_{TS})$ and $E_R(\mathbf{P}_R)$ are the electronic energies (molecular electrical properties) of the transition state and reactants, respectively.

For practical implementation of eq 3a, such expansion must be truncated. For instance, the truncation at the first term models the linear response of the barrier with respect to the EEF applied. Nevertheless, we can anticipate here that the neglect of the field-dependent nonlinear response of the barrier may lead to important quantitative or even qualitative errors in the predictions of the field-induced regioselectivity. Thus, the nonlinear terms are required to describe correctly the EEF effect on the energy barriers of chemical reactions. Conversely, the truncation of eq 3a at the third-order correction (given by $\boldsymbol{\beta}$) yields an expression flexible enough to properly evaluate the perturbation of the energy barriers induced by EEFs of any strength and direction at a low computational cost.

$$\Delta E^{\ddagger}(\mathbf{F}) = \Delta E^{\ddagger}(0) - \Delta\boldsymbol{\mu}^{\ddagger}\mathbf{F} - \frac{1}{2}\Delta\boldsymbol{\alpha}^{\ddagger}\mathbf{F}^2 - \frac{1}{6}\Delta\boldsymbol{\beta}^{\ddagger}\mathbf{F}^3 \tag{4}$$

Equation 4 is used throughout this work if not stated otherwise. It only requires the calculation of the field-free energy, $\boldsymbol{\mu}$, $\boldsymbol{\alpha}$, and $\boldsymbol{\beta}$ tensors for the reactants and transition states, which can be calculated analytically using several quantum chemistry packages. We refer to this approach to compute the FDB based on eq 4 as FDB_{β}. The benefits of including higher-order terms in eq 4 were also explored, but the changes in energy barrier due to the higher-order terms were usually below density functional theory (DFT) intrinsic errors. It is important to remark that the truncation at the linear term of eq 4 has been used in the literature to estimate the changes in the energy barriers induced by EEFs and light-emitting diodes (LEDs).[1c,5e,25]

The total electric polarizabilities and hyperpolarizabilities can be divided into the electronic contribution ($\mathbf{P}^{el}$), the nuclear relaxation (nr) contribution ($\mathbf{P}^{nr}$), and the curvature contribution ($\mathbf{P}^{curv}$).[26]

$$\mathbf{P} = \mathbf{P}^{el} + \mathbf{P}^{nr} + \mathbf{P}^{curv} \tag{5}$$

where $\mathbf{P}^{el}$ describes the response of the electrons to an external electric field at the equilibrium geometry, whereas $\mathbf{P}^{nr}$ and $\mathbf{P}^{curv}$ arise from the change of the electronic and vibrational energies due to the field-induced change of the equilibrium geometry and the shape of the potential energy surface (PES), respectively. The nuclear relaxation contribution contains all of the harmonic and lowest-order anharmonic terms, whereas the curvature contribution includes the rest of the higher-order vibrational anharmonicity. $\mathbf{P}^{curv}$ contribution is usually smaller than $\mathbf{P}^{el}$ and $\mathbf{P}^{nr}$, and far more expensive to compute, and it has not been evaluated in this work.[27]

Finally, it is worth noting that the field-induced changes in the thermodynamics of the reactions can be also easily computed and represented from an approximation homologous to FDB_{β}, expanding in a Taylor series the field-dependent reaction energies (for more details, see Figure SI8).

Scheme 1. Studied (3 + 2) Cycloaddition Reaction between Azomethine Ylide and Nitrostyrene with the Four Possible Cycloadducts

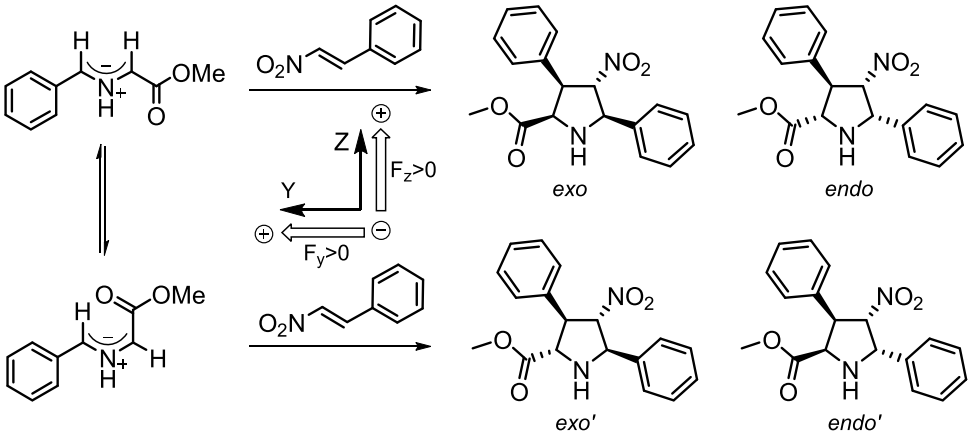

COMPUTATIONAL DETAILS

All electronic structure calculations have been performed using Gaussian16 software package.[28] For three studied cycloadditions, the geometries were optimized with the B3LYP exchange−correlation functional[29] using a 6-31+G(d,p) basis set[30] to span the atomic orbitals. Empirical dispersion corrections were added using the Grimme D3 correction[31] with Becke−Johnson damping factor.[32] Then, energy corrections, dipole moments, and (hyper)polarizabilities were obtained using the B3LYP functional and the 6-311+G(2d,2p) basis set, *i.e.*, B3LYP-D3BJ/6-311+G(2d,2p)//B3LYP-D3BJ/6-31+G(d,p). For the Diels−Alder cycloaddition between maleic anhydride and cyclopentadiene and to facilitate the direct comparison with the study of Shaik et al.,[4] the optimizations were performed using the BP86 functional,[33] *i.e.*, the computational level used for this reaction was B3LYP/6-311++G(d,p)//BP86/6-31+G(d). All stationary points on the potential energy surface (PES) were characterized through analytical vibrational frequency calculations.

To validate our approach, we have also computed the effect of explicit external static electric fields on the energy barriers. Several field strengths (F) were considered in the range $F = [-10^{-2},10^{-2}]$ au (1 au = 51.4 V·Å^{-1}) for all of the studied reactions; this range spans the order of magnitude of intrinsic LEF present in enzyme pockets or mitochondrial membrane interfaces.[34] It is important to remark that the positive direction of the electric field vector is defined from the negative to the positive charge, following the Gaussian16 convention (contrary to the conventional physics definition).[25] Notice that all of the calculations have been performed in the gas phase (for the solvent-phase electric field effect on a reaction, see the recent work of Dubey et al.[35]).

The field-free reactants were oriented by defining the z-axis as the reaction axis, *i.e.*, the axis along which the bonds are formed or broken. To avoid undesired field-induced rotations of the chemical systems during the geometry optimizations in the presence of explicit electric field, an in-house code was set up. The field-dependent equilibrium geometry is considered aligned to the original field-free equilibrium geometry when the rotation between them is smaller than 0.1° for the x, y, and z-axes. It is worth noticing that these constraints were added to ensure the formation of a reactant complex would correspond to an experimental scenario where one reactant is immobilized, for example, by being absorbed on a surface.[4,9f] The activation energy barriers for any strength and direction of the EEFs using the FDB$_\beta$ approach can be generated using an open-access script available at https://github.com/pau-besalu/FDB.

Preferably, the $\mathbf{P}^{nr}$ contribution should be computed at the same level of calculation as the electronic contribution. However, the energies and electronic contributions to the molecular electrical properties were computed using a triple-ζ basis (6-311++G(d,p) or 6-311+G(2d,2p)), while the equilibrium geometry and frequency calculations required to calculate the nuclear relaxation contribution were performed using a double-ζ basis (6-31+G(d,p)). Therefore, $\mathbf{P}^{nr}$ was computed using double-ζ basis, although we have checked that calculating $\mathbf{P}^{nr}$ with the triple-ζ basis leads to very similar results for the field-dependent energy barriers (for more details, see Table SI1).

RESULTS AND DISCUSSION

Initially, two 1,3-dipolar cycloadditions and one Diels−Alder (DA) cycloadditions involving small/medium-sized organic molecules are studied. For these first three reactions, the chemical barriers are computed using both FDB$_\beta$ and through the explicit optimization of equilibrium geometries of reactant complexes and TSs under EEF of several strengths and directions. After that, taking advantage of the computational benefits of the FDB$_\beta$ methodology, we have studied the DA cycloaddition between C_{60} fullerene and a diene. For this reaction, the determination of the geometries of reactant complexes and TSs under an electric field of several strengths and directions become computationally demanding. On the other hand, the FDB$_\beta$ methodology only requires the evaluation of field-free dipole moments and (hyper)-polarizabilities of the reactant complexes and TSs at their stationary points. Additionally, we introduce the two-dimensional (2D) representations[36] of the activation energy barriers, which allow the easy determination of the oriented EEF conditions requested to switch between kinetic control selectivities. In practice, this novel visual tool can "only" be generated using the FDB$_\beta$ methodology (otherwise, it becomes computationally prohibitive even for medium-sized systems).

Finally, another benefit of this research has been the analysis of the viability[37] of the oriented EEF as a synthetic strategy to obtain elusive cycloadducts. For instance, the exo′/endo′ cycloadducts in the (3 + 2) cycloadditions and the [5,6]-bond attack DA product between C_{60} and a diene.

(3 + 2) Cycloaddition between Azomethine Ylide and Nitrostyrene. The 1,3-dipolar cycloadditions, also known as Huisgen cycloadditions, have become a versatile route for the regio- and stereoselective construction of five-membered rings.[38] As the first test of our FDB$_\beta$ methodology, we selected the (3 + 2) cycloaddition between *N*-benzylidene-glycinate and *β*-nitrostyrene, which has been thoroughly studied both experimentally and computationally.[39] Depending on the experimental conditions, two ylides can be formed from the imide, yielding to four possible cycloadducts, namely, endo, exo, endo′, and exo′ (see Scheme 1). With usual heating and solvent, only the stereoisomers endo and exo are formed.[40] When the reaction is carried out without solvent, both in thermal or microwave conditions, a mixture of exo, endo, and endo′ cycloadducts is obtained.[40] Finally, the exo′ product has been synthesized catalyzing the reaction with consensus tetratricopeptide repeat proteins in tetrahydrofuran solution, which generates the four pyrrolidine stereoisomers in equimolar ratio.[41]

Our computational results for this reaction are fully consistent with previous studies.[40,41] Without the presence of an EEF, using a Boltzmann distribution over the activation energy barriers of the different cycloadducts obtained, the ratios 5.3:2.9:1.8:0 for the endo, exo, endo′, and exo′ are predicted, respectively.

Herein, the orientation of the nitrostyrene is fixed, and the two ylides are placed in the proper orientation to deliver each of the four possible cycloadducts. The *z*-axis is defined as the reaction axis; the olefinic double bond delimits the *y*-axis, and the direction where the phenyl group of the nitrostyrene is located indicates the positive region for both the *x* and *y*-axes (see Scheme 1).

Turning on an oriented EEF along the *z*-axis, the reaction can be either catalyzed or inhibited; see Figure 1. The field-induced catalysis/inhibition is controlled by the nucleophilicity−electrophilicity of the reactants triggered by the electronic density changes that the molecules suffer caused by the EE. As Shaik and co-workers have reported in several articles,[1c] the aforementioned field-induced changes in the electronic density are sometimes easily tracked by measuring the dipole moment of the transition-state geometries. For instance, for the endo pathway, when an EEF with $F_z > 0$ is applied, the reaction energy barrier decreases and the dipole moment module of the TS increases from 2.10 to 2.96 au. The increase in field-induced TS dipole moment illustrates the increase of the electron transfer from the highest occupied molecular orbital (HOMO) of the diene to the lowest unoccupied molecular orbital (LUMO) of the dienophile, which is the cause of the reduction of the cycloaddition activation barrier. The opposite is true when $F_z < 0$ is applied, and the dipole moment module of the TS decreases, resulting in an increase of the energy barrier. This rationalization can also be performed for all of the studied reactions (see Figures SI1 and SI2).

In Figure 1, for field strengths between -5×10^{-3} and 5×10^{-3} au, we found excellent agreement between the predictions obtained with the FDB$_\beta$ methodology and the results obtained reoptimizing the geometry of the reactants and TSs for each given value of EEFs. As expected, higher deviations are found using large field strengths, although the FDB$_\beta$ approach still provides reliable and fast estimations of the field-dependent energy barriers.

The four TSs present different polarities along the *y*-axis, and thus, this (3 + 2) cycloaddition may present electric-field-induced selectivity switches (EFISSs) when an EEF is placed along this axis. The activation energy barriers for all of the isomers, except exo′, increase when a positive or negative EEF is applied along the *y*-axis (Figure 2). Conversely, the energy barrier of the exo′ cycloadduct decreases (increases) for positive (negative) EEF. Then, for a $F_y = 5 \times 10^{-3}$ au, an EFISS occurs and the elusive exo′ cycloadduct can be achieved as the major product. Consequently, at 120 °C, the aforementioned field-free 5.3:2.9:1.8:0 ratio for the endo, exo, endo′, and exo′ cycloadducts, respectively, completely switches into 0.1:0.1:0:9.8 at $F_y = 1 \times 10^{-2}$ au. Additionally, the oriented EEF along the *x*-axis also presents some interesting reactivity features (see Figure SI3). For instance, for $F_x > 0$, the endo (major product under free-field

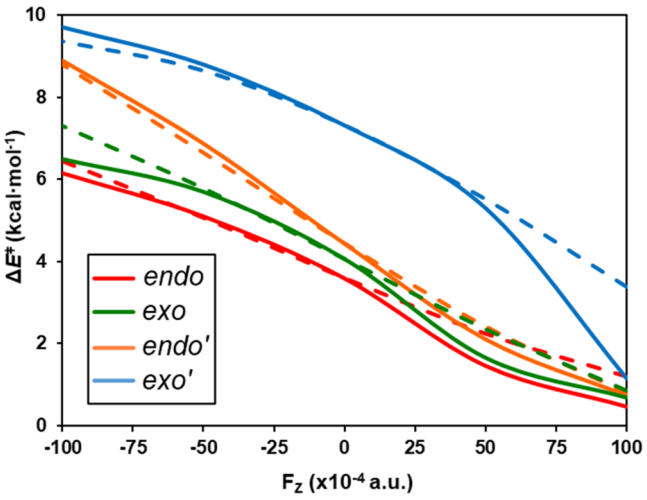

Figure 1. Activation energy barriers for the (3 + 2) cycloaddition between azomethine ylide and nitrostyrene (kcal·mol^{-1}) in terms of the applied EEF *z*-axis. Dashed lines represent the prediction using FDB$_\beta$. Solid lines correspond to the explicit optimization of the reactants, products, and TSs in the presence of an EEF. Calculations were performed at the B3LYP-D3BJ/6-311+G(2d,2p)//B3LYP-D3BJ/6-31+G(d,p) level of theory.

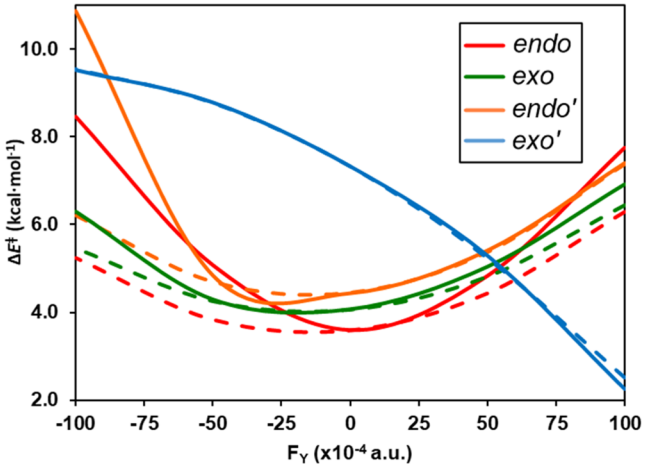

Figure 2. Activation energy barriers for the (3 + 2) cycloaddition between azomethine ylide and nitrostyrene (kcal·mol^{-1}) in terms of the applied EEF *y*-axis. See Figure 1 caption for additional details.

-19×10^{-4} au, an EFISS occurs between the activation energy barriers of the endo and exo (the second major product under free-field conditions) cycloadducts, which leads to an exo selectivity. Then, the oriented EEF could be used for the regio- and stereo-controlled synthesis of the five-membered rings obtained from 1,3-dipolar cycloadditions.

From a computational cost point of view, the evaluation of the kinetic barriers for four regioisomers with N EEFs of different strengths and orientations (positive and negative) along all three directions of space implies the optimization of $24N + 8$ stationary points. On the other hand, using the FDB_β methodology, the same information can be generated computing only the corresponding electrical properties of the field-free reactants and TSs stationary points. Thus, using the FDB_β methodology, $24N$ optimization of the geometry of the field-dependent stationary points is avoided, implying a considerable computational reduction cost. Nevertheless, it is important to note that the FDB_β approach considers that the same reaction mechanism holds for any combination of EEF strengths placed in the x, y, and z-axes. For instance, it does not take into account the possibility that a concerted cycloaddition mechanism can become a stepwise process. The stabilization of the zwitterionic or radical intermediate and the mechanistic crossover usually occur with strong oriented EEF. In these situations, the valence bond model can be a useful tool to provide physical insight to rationalize the mechanistic crossover.[1c,2S]

Figure 3 illustrates the accuracy obtained using different possible truncations of eq 4 for the exo cycloadduct in terms of

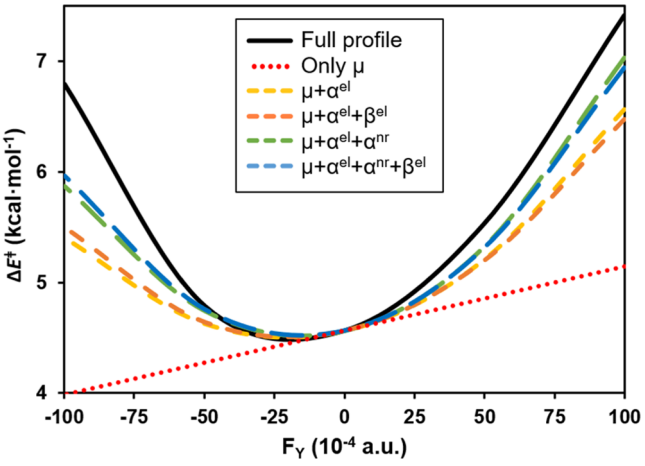

Figure 3. Activation energy barriers for the (3 + 2) cycloaddition between azomethine ylide and nitrostyrene (kcal·mol^{-1}) for the exo cycloadduct in terms of y-axis EEF. Dotted and dashed lines represent several levels of truncation of eq 4. See Figure 1 caption for additional details.

the strength of a y-axis EEF. The consideration of only the linear term leads to a wrong prediction of the activation barrier in the presence of F_y, which shows a clear nonlinear dependence. However, it is worth noting that the absolute errors are <3 kcal·mol^{-1} (see Figure SI4). The incorporation of α^{el} into the model improves substantially the prediction, and a reasonable semiquantitative picture is already obtained. In this particular case, the improvement of the β^{el} term in the Taylor series is negligible. Nevertheless, we recommend including this term routinely in the Taylor series, especially, when α and β can be analytically calculated with an acceptable computational cost.

Up to this point, only electronic terms were considered in the definition of μ, α, and β of eq 4. However, the inclusion of nuclear relaxation (nr) contribution to α leads to an improved description of the field-dependent barriers, reducing the error down to <0.5 kcal·mol^{-1} (see Figures 3 and SI4). Thus, and as expected, a progressive and systematic enhancement of the prediction can always be achieved owing to the addition of new terms to the Taylor expansion. As an illustrative example, at $F_y = -5 \times 10^3$ au, the individual percentage contributions to the activation barrier energy for the μ, α^{el}, α^{nr}, and β terms are −150, 184, 60, and 6%, respectively (see Figure SI5).

As a method based on the Taylor expansion, the FDB_β approximation validity is reduced when the EEF strength increases. Nevertheless, the studies of the reactivity and selectivity induced by EEF often use intensities of the electric fields below 1000 mV·Å^{-1}. Usually, the energy barrier discrepancies between the optimized EEF and the FDB_β approach could be attributed to the nuclear relaxation of the TSs and reactant complexes, which may be partially taken into account by the FDB_β approach including the nuclear relaxation contribution to the polarizability in the Taylor expansion. An indication of the nuclear relaxation relevance is given by the presence of low frequencies in the infrared spectrum.

Overall, the FDB_β approximation including only the electronic contributions to of μ, α, and β provides a mean error for activation energy barriers of all four cycloadducts lower than 1.0 kcal·mol^{-1}. Therefore, this methodology has been selected to study the field-catalyzed reactivity throughout this work.

Diels−Alder Reaction between Maleic Anhydride and Cyclopentadiene. In 1928, Diels and Alder' seminal work[42] introduces the (4 + 2) cycloaddition between 1,3-dienes and a substituted alkene, the Diels−Alder (DA) reaction. This cycloaddition allows the regio- and stereo-controlled synthesis of cyclohexene derivatives.[43] One of the archetypal DA cycloadditions is the reaction between maleic anhydride and cyclopentadiene (Scheme 2).[44] For this reaction, the effects of

Scheme 2. Studied DA Reaction between Maleic Anhydride and Cyclopentadiene

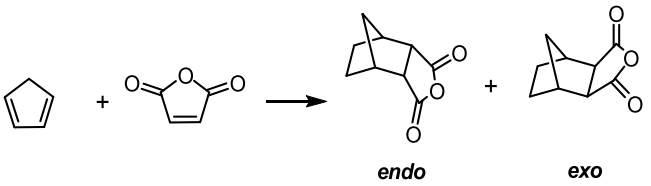

oriented EEFs have thoroughly been studied both from theoretical[4,4S] and experimental[3d] points of view. Then, for comparison purposes, this reaction has been selected to check the FDB_β performance and to introduce the 2D representation of the chemical barriers for the kinetic product of the reaction.

As Shaik and co-workers reported,[4] under free-field conditions, the formation of both endo and exo cycloadducts is exergonic by −15.4 and −16.1 kcal·mol^{-1}, respectively, and the activation energy barriers for the formation of these products are 15.5 and 16.7 kcal·mol^{-1}, respectively. Assuming that the reaction is kinetically driven, the endo cycloadduct is obtained as the major product under free-field conditions.

In a similar way to the previous example, applying an EEF along the reaction axis (z-axis) catalyzes ($F_z < 0$) or inhibits ($F_z > 0$) the endo and exo pathways (Figure 4). At large F_z

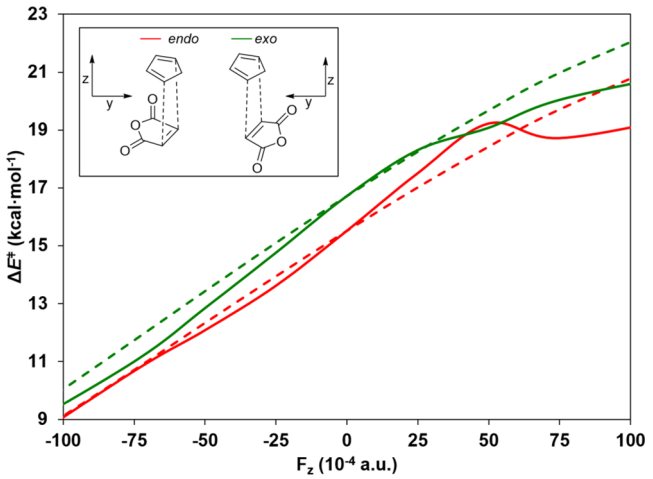

Figure 4. Activation energy barriers for the endo and exo DA pathways between maleic anhydride and cyclopentadiene (kcal·mol^{-1}) in terms of z-axis EEF. Calculations performed at the B3LYP/6-311++G(d,p)//BP86/6-31+G(d) level of theory. See Figure 1 caption for additional details.

strengths, the energy barrier discrepancies found between the optimized EEF and the FDB$_\beta$ approximation are due to the stabilization of a zwitterionic intermediate.[4] If a y-axis EEF is applied, an EFISS is found at $F_y \leq -5 \times 10^{-3}$ au (0.257 V·Å^{-1} or 1.29×10^{12} W·cm^{-2}), where the DA reaction presents exo selectivity (Figure 5). The endo barrier is barely affected within

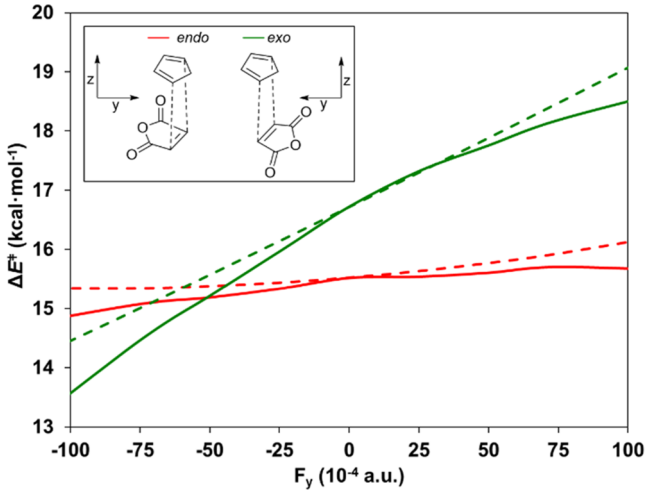

Figure 5. Activation energy barriers for the endo and exo DA cycloaddition between maleic anhydride and cyclopentadiene (kcal·mol^{-1}) in terms of y-axis EEF. See Figure 4 caption for additional details.

the scanned range of electric field strengths, whereas the exo one is modified by almost 6 kcal·mol^{-1}. As reported elsewhere,[46] the secondary orbital interactions (SOI) play a key role in the endo product stabilization at free field. At $F_y \leq 0$ au, the destabilization of the endo product with respect to the exo occurs due to the energy increase of the orbital responsible for the stabilizing SOI (for more details, see Figure SI6 and the discussion therein). For this reaction, the FDB$_\beta$ approach also presents a robust performance, *i.e.*, the mean absolute error (MAE) with respect to the energy profile obtained optimizing with explicit EEFs is <1 kcal·mol^{-1} and the maximum error is <2 kcal·mol^{-1}.

Taking advantage of the low FDB$_\beta$ computational cost, it is possible to generate 2D representations summarizing the effects of the combination of any strength of the y- and z-axis EEFs (Figure 6). The red (green) region corresponds to the

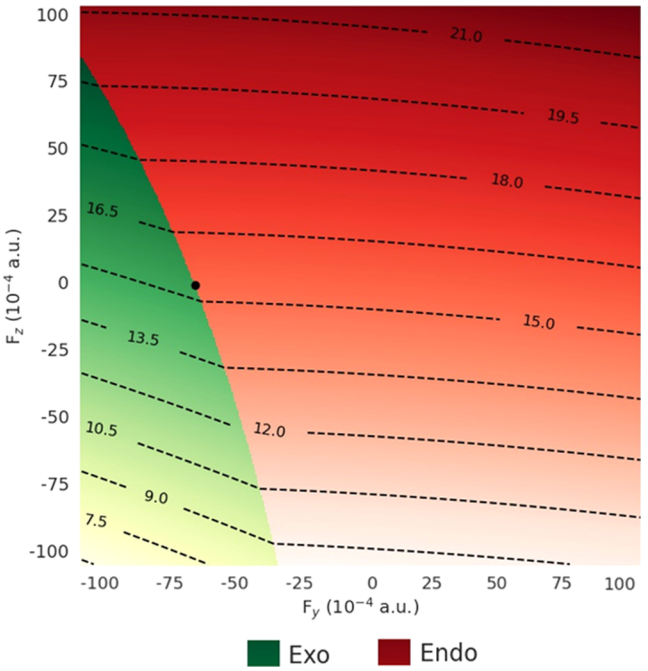

Figure 6. Two-dimensional representation of the chemical barriers for the major kinetic product of the DA reaction between maleic anhydride and cyclopentadiene in terms of EEFs along the y and z-axes using the FDB$_\beta$ approach. Green and red zones indicate exo and endo kinetic selectivities, respectively. Calculations are performed at the B3LYP/6-311++G(d,p)//BP86/6-31+G(d) level of theory. Isoenergy barrier lines in kcal·mol^{-1}.

range of F_z and F_y for which the endo (exo) barrier is lower than the exo (endo) barrier. The intensity of the color and the isocontour lines indicate the magnitude of the activation energy barriers of the kinetically most favored reaction in kcal·mol^{-1}. Isocontour lines are not equidistant, indicating a nonlinear dependence of the chemical barrier with respect to EEF. For the same reason, the border from endo to exo selectivity regions is not linear (see Figure SI7 for the 2D representation using only the linear μ term in eq 4).

In addition, it is worth noting that the endo energy barriers are barely affected by the value of F_y (in agreement with Figure 5), as expected considering the small dipole moment along the y-axis of the endo TS structure.

From this 2D representation, it is also possible to define some novel reactivity EEF concepts. For instance, the EFISS curve defines the set of all vectors that switch the selectivity. In this particular case, the EFISS curve is given by all (F_y,F_z) vectors that switch from endo to exo selectivities. Additionally, it is possible to determine the vector with the minimum module within the set, MEFISS. In Figure 6, MEFISS is represented as a black dot at $F_z = 0$ au and $F_y = -5.8 \times 10^{-3}$ au. Another important point to remark is that the three-

dimensional (3D) representations are also easy to achieve, for instance, performing several (F_y,F_z) 2D plots with different constant F_x values (for an illustrative example, see Figure SI8).

To catalyze or inhibit a reaction, usually, the most relevant orientation is the reaction coordinate.[47] However, the reaction pathways can become quite complex and their regioselectivity, stereoselectivity, and enantioselectivity cannot be controlled by placing the electric field in only one direction. For these systems, the 2D and 3D representations using the FDB$_\beta$ approach are valuable tools to predict the electric-field-induced reactivity. Additionally, external electric fields can be used to simulate the local electric fields induced by charged functional groups and metal ions, which increases the reaction rate and controls the selectivity of organocatalytic reactions catalyzed by enzymes and zeolites.[1]

Representing these 2D (or 3D) plots using explicit field-dependent optimizations of the reactants and TSs requires an enormous computational cost. For instance, the optimization of $(4N)^2 + 4$ field-dependent stationary points is required to plot the corresponding version of Figure 6, where N is the number of selected EEF strengths (positive and negative). On the other hand, using the FDB$_\beta$ approximations, representing Figure 6 only requires the optimization of four field-free stationary points and the calculation of their corresponding electrical properties, which implies a $(4N^2 + 1)$-fold computational cost reduction. In addition, here, is important to remark that for such kind of 2D plots, N should be somewhat large to obtain an acceptable resolution.

Finally, the representation of the homologous eq 4 but expanding in a Taylor series, the field-dependent reaction energies instead of the energy barriers shows that the exothermicity of both reactions (endo and exo) increases for the same EEFs for which the corresponding energy barrier decreases, *i.e.*, $F_z < 0$ (see Figure SI9). Thus, the relationship between field-dependent kinetics and thermodynamics follows the trend given by the Bell−Evans−Polanyi principle.[48]

(3 + 2) Cycloaddition between Methoxyethene and Phenyl Diazomethane. As another example to illustrate the potential of the FDB$_\beta$ approach, we select a (3 + 2) cycloaddition for which oriented EFFs are potentially able to tune the selectivity between four possible cycloadducts (endo, endo′, exo, and exo′). For this purpose, we choose as reactants a 1,3-diene and a dipolarophile with clear polar characters, *i.e.*, the 1,3-dipolar reaction between phenyl diazomethane and methyl vinyl ether (Scheme 3). The molecular orientation is defined as follows: z-axis was set to be the reaction axis, y-axis to be parallel to the olefin double bond and positive in the direction of the methoxy substituent, and the x-axis is negative in the zone where the methoxy group is located.

Scheme 3. Studied 1,3-Dipolar Cycloaddition between Phenyl Diazomethane and Methoxyethene and the Four Possible Cycloadducts; Definition of the Cartesian Coordinates for the Reaction

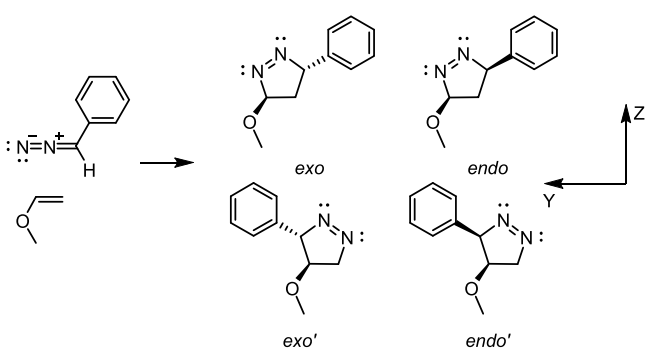

Under free-field conditions, the exo pathway presents the lowest activation energy barrier (19.8 kcal·mol^{-1}), while the endo, exo′, and endo′ pathways are located at 0.2, 1.4, and 1.7 kcal·mol^{-1} above it, respectively. Then, at room temperature, the four cycloadducts present the 5.4:3.8:0.5:0.3 (exo/endo/exo′/endo′) ratios.

For $F_x > 0$, the endo kinetic selectivity is enhanced, whereas the activation energy barriers increase for the other regioisomers (Figure 7). On the contrary, for $0 > F_x > -6.2 \times 10^{-3}$ au, the exo energy barrier is the lowest one, whereas exo′ cycloadduct becomes the kinetic product of the reaction for $F_x < -6.2 \times 10^{-3}$ au. In this manner, only by varying the intensity of the EEF in the x-axis, one achieves as the major product the endo, exo, or exo′ cycloadducts, passing through two different EFISSs along the path.

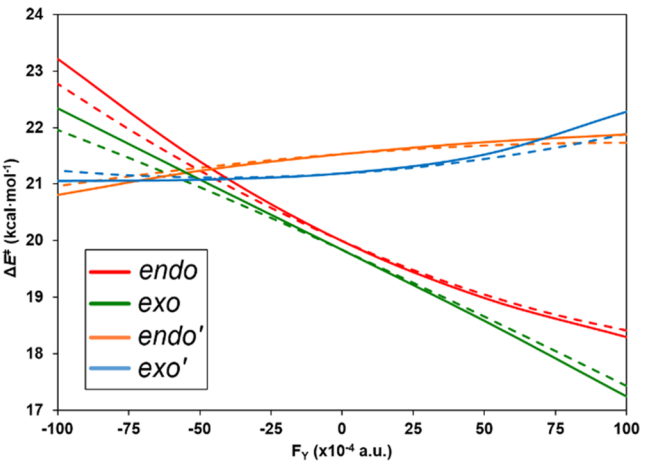

Figure 7. Activation energy barriers for (3 + 2) dipolar reactions between phenyl diazomethane and methoxyethene (kcal·mol^{-1}) in terms of the applied x-axis EEF. See Figure 1 caption for additional details.

For $F_y > 0$, the exo selectivity is enhanced with respect to endo pathway (Figure 8), whereas the change with respect to the strength of the EEF of endo′ and exo′ activation energy barriers is very small. On the other hand, for $F_y < 0$, the endo and exo pathways are inhibited, and then at $F_y = -10^2$ au, the endo′ and exo′ become the only kinetically feasible cycloadducts. Finally, the EEF along the reaction axis (F_z) catalyzes or inhibits the endo and exo pathways in a similar way (for more details, see Figure SI10).

A visual summary 2D representation of the activation energy barriers for the major kinetic cycloadduct using any combination of any F_x and F_y strengths is displayed in Figure 9. Under field-free conditions, the exo and endo energy barriers are almost isoenergetic and present the lowest activation energy barriers. From a general perspective, the exo selectivity can be enhanced by negative F_x and positive F_y. The kinetic endo selectivity can be obtained using positive F_x. On the other hand, using negative F_x and F_y electric fields, the major kinetic cycloadduct becomes the exo′ product. Finally, the endo′ cycloadduct, which is the most elusive product under field-free conditions, can be obtained as a major kinetic

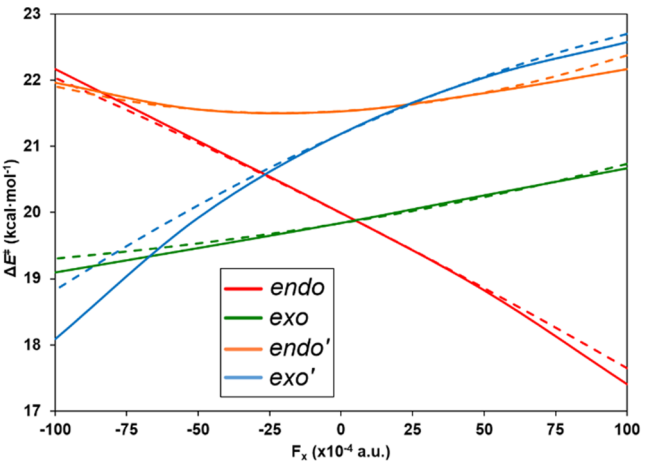

Figure 8. Activation energy barriers for the (3 + 2) dipolar reaction between phenyl diazomethane and methoxyethene (kcal·mol^{-1}) in terms of the applied *y*-axis EEF. See Figure 1 caption for additional details.

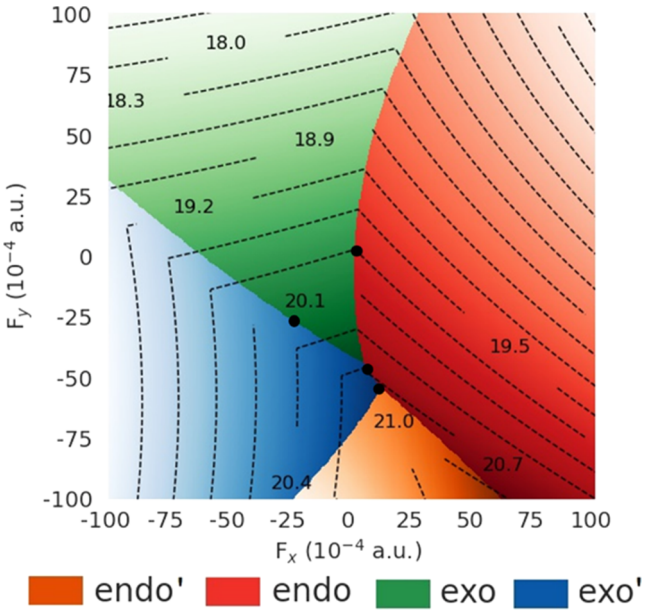

Figure 9. Two-dimensional representation of the activation energy barriers for the major kinetic product of the (3 + 2) dipolar reaction between phenyl diazomethane and methoxyethene in terms of the applied EEFs along the *x*- and *y*-axes using the FDB$_\beta$ approach. Green, red, blue, and orange zones indicate exo, endo, exo′, and endo′ kinetic selectivities, respectively. Black dots indicate the MEFISS points. Calculations are performed at the B3LYP-D3BJ/6-311+G(2d,2p)//B3LYP-D3BJ/6-31+G(d,p) level of theory. Isoenergy barrier lines in kcal·mol^{-1}.

product applying $F_y < -5.0 \times 10^{-3}$ au and moderate positive F_x.

Figure 9 also shows five EFISS curves corresponding to the exo/endo, exo/exo′, endo/endo′, endo/exo′, and exo′/endo′ selectivity switches and four MEFISSs (indicated as black dots). Herein, it is important to underline that the exo, endo, exo′, and endo′ selectivities can be tuned at will using relatively small EEF window values, *i.e.*, $-25 \times 10^{-4} < F_x < 10^{-4}$ and $-60 \times 10^{-4} < F_y < 0$ au. Additionally, the 2D plot generated with the FDB$_\beta$ approach also illustrates that the dependence of the barriers in terms of the strength of the applied EEF is nonlinear (see also Figure SI11) since both the displayed isocontour lines and the EFISS curves are not straight lines.

As in the previous example, it is also possible to generate several (F_x,F_y) 2D plots with different constant F_z strengths. As indicated previously, the EEF along the reaction coordinate modifies the magnitude of the activation energy barrier (catalyze or inhibit) but not the selectivity. Consequently, not relevant differences are found with respect to Figure 9 (see Figure SI12). Again, it is important to remark that the generation of Figure 9 using explicit field-dependent equilibrium geometry optimizations requires the calculation of $(8N)^2 + 8$ stationary points, where N is the number of selected positive and negative EEF strengths. On the other hand, the FDB$_\beta$ approximations only requires the optimization of eight field-free stationary points and the calculation of their corresponding electrical properties. Therefore, for a reaction with four possible products, FDB$_\beta$ is $(8N^2 + 1)$-fold cheaper in terms of CPU time than the usual methodology. A detailed summary of the computational cost benefits of the FDB$_\beta$ approximation can be found in Table SI2.

Diels–Alder Reaction between C_{60} and Cyclopentadiene. As a last example, we select a reaction involving 65 carbon atoms, the DA reaction between C_{60} fullerene and cyclopentadiene.[49] Under field-free conditions, the energy barrier of this DA cycloaddition is lower for [6,6]- than for [5,6]-bonds (Scheme 4).[50] The Diels–Alder [5,6] functionalization has never been reported experimentally for the DA cycloadditions to C_{60}, although theoretically it was found possible in highly reduced C_{60}[51] or in the high-spin states of C_{60}.[52] Herein, we explore the potential of the oriented EEF as a synthetic strategy to obtain the elusive [5,6]-bond cycloadduct.

Scheme 4. Schematic Representation of DA Reaction over a [6,6]- (Top) or [5,6]-Bond (Bottom) of a C_{60} Fullerene Represented by One of Its Corannulene Unit, Respectively

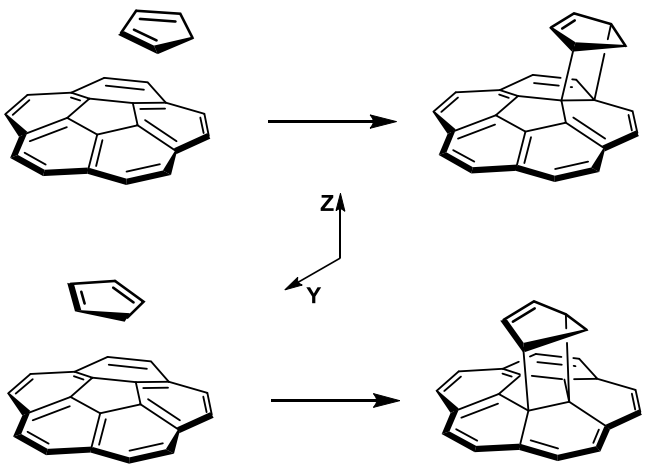

The reactant complex is oriented so that the *z*-axis is parallel to the reaction coordinate, and either the attacked [5,6]- or the [6,6]-bond defines the *y*-axis (Scheme 4). The reactivity is almost not changing when an EEF is applied either along the *x*- or *y*-axis (see Figures SI13 and S14 for more details); therefore, only the *z*-axis results are discussed herein. For $F_z > 0$ ($F_z < 0$) au, the FDB$_\beta$ approach predicts that the activation energy barriers are increasing (decreasing) for both pathways (Figure 10). The role of the EEF on this reaction can be

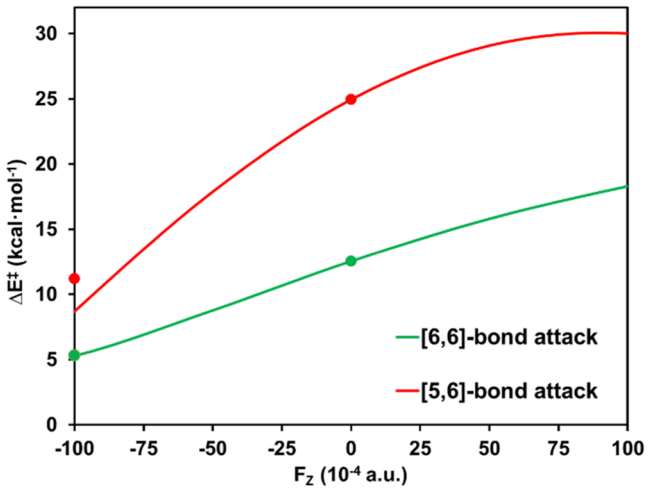

Figure 10. Activation energy barriers of the DA between C_{60} and cyclopentadiene (kcal·mol^{-1}) in terms of the applied *z*-axis EEF. Solid lines are calculated at the B3LYP-D3BJ/6-311+G(2d,2p)//B3LYP-D3BJ/6-31+G(d,p) level of theory using the FDB$_\beta$ approximation. Color dots correspond to explicit field-dependent geometrical optimizations performed for a specific EEF.

rationalized by analyzing the effect of the electric field on the HOMO and LUMO. The presence of a negative (positive) pole of the EEF located above (below) the diene (C_{60}) destabilizes (stabilizes) the HOMO (LUMO) mainly located in the cyclopentadiene (C_{60}), which favors the reaction and then decreases the energy barrier.

For $F_z < 0$, the decrease of the activation energy barriers is more pronounced for the [5,6]-bond than for the [6,6]-bond pathway, implying a reduction of the gap between the two activation barriers, although no EFISS is observed in the studied range. At $F_z = 10^{-2}$ au, the FDB$_\beta$ approach estimates a gap difference between both pathways of only 3 kcal·mol^{-1}, a reduction of 9 kcal·mol^{-1} with respect to the free-field conditions. To check the validity of this conclusion, optimizations of the reactants and TSs at $F_z = -10^{-2}$ au were performed. The results displayed in Figure 10 confirm the FDB$_\beta$ results, although there is a difference of 2.5 kcal·mol^{-1} between the difference in the energy barriers obtained with both methodologies. Thus, we conclude that for $F_z < -10^{-2}$ au and high temperatures, some traces of the [5,6]-cycloadduct in the product mixture could be found.

CONCLUSIONS

A novel methodology to estimate activation energy barriers in the presence of external electric fields (EEFs) is reported herein. The FDB$_\beta$ approach is based on the Taylor expansion of the field-dependent energy of the reactants and transition states (TSs) in terms of their dipole moments and electrical (hyper)polarizabilities. As illustrative examples, to assess the reliability and validity of the proposed method, we have studied the effect of EEFs on four reactions (two 1,3-dipolar and two Diels–Alder cycloadditions).

The FDB$_\beta$ approach only requires the geometry optimizations of the reactants and TSs under free-field conditions, and the calculation of their (hyper)polarizabilities. Thus, no explicit EEF calculations are required. The obtained results indicate that estimations of the activation energy barriers for different EEF strengths can be obtained with errors usually smaller than 1 kcal·mol^{-1}. Additionally, the consideration of only the electronic contribution to the electrical (hyper)polarizabilities is sufficient to recover most of the changes in the activation energy barriers. Nevertheless, if it is required, the inclusion of nuclear relaxation contribution to the polarizability, which can be obtained from a single frequency calculation, further improves the quality of the energy barrier estimations.

The benefits of the FDB$_\beta$ methodology are its simplicity and the massive reduction of the CPU-time cost with respect to the explicit optimizations of the reactant complexes and transition states for several EEF strengths. The FDB$_\beta$ approach permits systematic 1D, 2D, and 3D representations of the activation energy barriers for any strength and direction of the EEFs. Furthermore, one can determine which is the optimum strength and direction of an EEF required to induce a particular selectivity switch. Thus, the FDB$_\beta$ approach can be used to "seek and identify" the potential synthesis using EEF of elusive regioisomers, which cannot be obtained under other experimental conditions. For instance, for the studied 1,3-dipolar reaction between methoxyethene and phenyl diazomethane, the four possible cycloadducts can be obtained as major kinetic control products by changing only the magnitudes and directions of F_x and F_y.

To conclude, we believe that the FDB$_\beta$ approach can be used as a fast-screening tool to predict novel potential field-induced catalysis and regioselectivities, especially for systems of organocatalytic and biocatalytic interests that involve a large number of atoms.

ASSOCIATED CONTENT

Supporting Information

The Supporting Information is available free of charge at https://pubs.acs.org/doi/10.1021/acscatal.1c04247.

Nuclear relaxation contribution assessment; dipole moment changes in TS structures; MAE for several FDB approaches; 1D representations of the EEF-induced chemical barriers for the remaining directions and cycloadditions indicated but not reported in the manuscript; DA secondary orbital interaction analysis; 2D maps for different FDB approaches and for several F_z EEFs for the DA maleic anhydride and cyclopentadiene and the (3 + 2) cycloaddition between azomethine ylide and nitrostyrene; CPU time required using the explicit optimization of reactant complexes and transition states in the presence of an EEF and using the FDB$_\beta$ approach; and Cartesian coordinates (PDF)

AUTHOR INFORMATION

Corresponding Authors

Josep M. Luis − *Institut de Química Computacional i Catàlisi and Departament de Química, Universitat de Girona, 17003 Girona, Catalonia, Spain;* orcid.org/0000-0002-2880-8680; Email: josepm.luis@udg.edu

Miquel Torrent-Sucarrat − *Department of Organic Chemistry I, Centro de Innovación en Química Avanzada (ORFEO-CINQA), Universidad del País Vasco/Euskal Herriko Unibertsitatea (UPV/EHU) and Donostia International Physics Center (DIPC), E-20018 Donostia/San Sebastián, Euskadi, Spain; Ikerbasque, Basque Foundation for Science, 48009 Bilbao, Euskadi, Spain;* orcid.org/0000-0003-2689-0278; Email: miqueltorrentsucarrat@gmail.com

Pau Besalú-Sala − *Institut de Química Computacional i Catàlisi and Departament de Química, Universitat de Girona, 17003 Girona, Catalonia, Spain;* orcid.org/0000-0002-0955-9762

Miquel Solà − *Institut de Química Computacional i Catàlisi and Departament de Química, Universitat de Girona, 17003 Girona, Catalonia, Spain;* orcid.org/0000-0002-1917-7450

Complete contact information is available at: https://pubs.acs.org/10.1021/acscatal.1c04247

Author Contributions

M.T.-S., M.S., and J.M.L. devised and supervised the project. P.B-S. performed all calculations and analyzed the results. The manuscript was written through the contributions of all authors. All authors approved the final version of the manuscript.

Notes

The authors declare no competing financial interest.

■ ACKNOWLEDGMENTS

This work was supported with funds from the Ministerio de Economía y Competitividad (MINECO) of Spain (project CTQ2017-85341-P to M.S.), the Spanish government MICINN (projects PGC2018-098212-B-C22 to J.M.L, PID2020-113711GB-I00 to M.S., and PID2019-104772GB-I00 to M.T.S.), the Generalitat de Catalunya (project 2017SGR39 to M.S. and J.M.L.), and Gobierno Vasco (project IT1346-19 to M.T.S.). The authors thank the Spanish government for the predoctoral grant to P.B.-S. (FPU17/02058). They are also grateful for the computational time financed by the Consorci de Serveis Universitaris de Catalunya (CSUC). They thank the reviewers for their comments and helpful suggestions.

■ REFERENCES

(1) (a) Shaik, S.; Mandal, D.; Ramanan, R. Oriented Electric Fields as Future Smart Reagents in Chemistry. *Nat. Chem.* **2016**, *8*, 1091−1098. (b) Che, F.; Gray, J. T.; Ha, S.; Kruse, N.; Scott, S. L.; McEwen, J.-S. Elucidating the Roles of Electric Fields in Catalysis: A Perspective. *ACS Catal.* **2018**, *8*, 5153−5174. (c) Shaik, S.; Ramanan, R.; Danovich, D.; Mandal, D. Structure and Reactivity/Selectivity Control by Oriented-External Electric Fields. *Chem. Soc. Rev.* **2018**, *47*, 5125−5145. (d) Robertson, J. C.; Coote, M. L.; Bissember, A. C. Synthetic Applications of Light, Electricity, Mechanical Force and Flow. *Nat. Rev. Chem.* **2019**, *3*, 290−304. (e) Shaik, S.; Danovich, D.; Joy, J.; Wang, Z.; Stuyver, T. Electric-Field Mediated Chemistry: Uncovering and Exploiting the Potential of (Oriented) Electric Fields to Exert Chemical Catalysis and Reaction Control. *J. Am. Chem. Soc.* **2020**, *142*, 12551−12562. (f) Léonard, N. G.; Dhaoui, R.; Chantarojsiri, T.; Yang, J. Y. Electric Fields in Catalysis: From Enzymes to Molecular Catalysts. *ACS Catal.* **2021**, 10923−10932.

(2) (a) Bhattacharyya, D.; Videla, P. E.; Cattaneo, M.; Batista, V. S.; Lian, T.; Kubiak, C. P. Vibrational Stark Shift Spectroscopy of Catalysts under the Influence of Electric Fields at Electrode−Solution Interfaces. *Chem. Sci.* **2021**, *12*, 10131−10149. (b) Concellón, A.; Lu, R.-Q.; Yoshinaga, K.; Hsu, H.-F.; Swager, T. M. Electric-Field-Induced Chirality in Columnar Liquid Crystals. *J. Am. Chem. Soc.* **2021**, *143*, 9260−9266. (c) Kawasaki, T.; Kaimori, Y.; Shimada, S.; Hara, N.; Sato, S.; Suzuki, K.; Asahi, T.; Matsumoto, A.; Soai, K. Asymmetric Autocatalysis Triggered by Triglycine Sulfate with Switchable Chirality by Altering the Direction of the Applied Electric Field. *Chem. Commun.* **2021**, *57*, 5999−6002. (d) Nakamura, K.; Sugiura, S.; Araoka, F.; Aya, S.; Takanishi, Y.; Watanabe, G.; Sato, R.; Shigeta, Y.; Maeda, H. Conformation-Changeable π-Electronic Systems with Metastable Bent-Core Conformations and Liquid-Crystalline-State Electric-Field-Responsive Properties. *Org. Lett.* **2021**, *23*, 305−310. (e) Yu, Z.; Wang, L.; Mu, X.; Chen, C.-C.; Wu, Y.; Cao, J.; Tang, Y. Intramolecular Electric Field Construction in Metal Phthalocyanine as Dopant-Free Hole Transporting Material for Stable Perovskite Solar Cells with >21% Efficiency. *Angew. Chem., Int. Ed.* **2021**, *60*, 6294−6299.

(3) (a) Suydam, I. T.; Snow, C. D.; Pande, V. S.; Boxer, S. G. Electric Fields at the Active Site of an Enzyme: Direct Comparison of Experiment with Theory. *Science* **2006**, *313*, 200−204. (b) Gorin, C. F.; Beh, E. S.; Kanan, M. W. An Electric Field−Induced Change in the Selectivity of a Metal Oxide−Catalyzed Epoxide Rearrangement. *J. Am. Chem. Soc.* **2012**, *134*, 186−189. (c) Gorin, C. F.; Beh, E. S.; Bui, Q. M.; Dick, G. R.; Kanan, M. W. Interfacial Electric Field Effects on a Carbene Reaction Catalyzed by Rh Porphyrins. *J. Am. Chem. Soc.* **2013**, *135*, 11257−11265. (d) Aragonès, A. C.; Haworth, N. L.; Darwish, N.; Ciampi, S.; Bloomfield, N. J.; Wallace, G. G.; Diez-Perez, I.; Coote, M. L. Electrostatic Catalysis of a Diels−Alder Reaction. *Nature* **2016**, *531*, 88−91. (e) Olavarría-Contreras, I. J.; Etcheverry-Berríos, A.; Qian, W.; Gutiérrez-Cerón, C.; Campos-Olguín, A.; Sañudo, E. C.; Duli, D.; Ruiz, E.; Aliaga-Alcalde, N.; Soler, M.; van der Zant, H. S. J. Electric-Field Induced Bistability in Single-Molecule Conductance Measurements for Boron Coordinated Curcuminoid Compounds. *Chem. Sci.* **2018**, *9*, 6988−6996. (f) Huang, X.; Tang, C.; Li, J.; Chen, L.-C.; Zheng, J.; Zhang, P.; Le, J.; Li, R.; Li, X.; Liu, J.; Yang, Y.; Shi, J.; Chen, Z.; Bai, M.; Zhang, H.-L.; Xia, H.; Cheng, J.; Tian, Z.-Q.; Hong, W. Electric Field−Induced Selective Catalysis of Single-Molecule Reaction. *Sci. Adv.* **2019**, *5*, No. eaaw3072. (g) Zang, Y.; Zou, Q.; Fu, T.; Ng, F.; Fowler, B.; Yang, J.; Li, H.; Steigerwald, M. L.; Nuckolls, C.; Venkataraman, L. Directing Isomerization Reactions of Cumulenes with Electric Fields. *Nat. Commun.* **2019**, *10*, No. 4482. (h) Tang, Y.; Zhou, Y.; Zhou, D.; Chen, Y.; Xiao, Z.; Shi, J.; Liu, J.; Hong, W. Electric Field-Induced Assembly in Single-Stacking Terphenyl Junctions. *J. Am. Chem. Soc.* **2020**, *142*, 19101−19109. (i) Gao, T.; Pan, Z.; Cai, Z.; Zheng, J.; Tang, C.; Yuan, S.; Zhao, S. q.; Bai, H.; Yang, Y.; Shi, J.; Xiao, Z.; Liu, J.; Hong, W. Electric Field-Induced Switching among Multiple Conductance Pathways in Single-Molecule Junctions. *Chem. Commun.* **2021**, *57*, 7160−7163.

(4) Meir, R.; Chen, H.; Lai, W.; Shaik, S. Oriented Electric Fields Accelerate Diels−Alder Reactions and Control the endo/exo Selectivity. *ChemPhysChem* **2010**, *11*, 301−310.

(5) (a) Andrés, J. L.; Lledós, A.; Duran, M.; Bertrán, J. Electric Fields Acting as Catalysts in Chemical Reactions. An ab Initio Study of the Walden Inversion Reaction. *Chem. Phys. Lett.* **1988**, *153*, 82−86. (b) Carbonell, E.; Duran, M.; Lledós, A.; Bertrán, J. Catalysis of Friedel-Crafts Reactions by Electric Fields. *J. Phys. Chem. A.* **1991**, *95*, 179−183. (c) Bhattacharyya, K.; Karmakar, S.; Datta, A. External electric field control: driving the reactivity of metal-free azide−alkyne click reactions. *Phys. Chem. Chem. Phys.* **2017**, *19*, 22482−22486. (d) Gryn'ova, G.; Coote, M. L. Directionality and the Role of Polarization in Electric Field Effects on Radical Stability. *Aust. J. Chem.* **2017**, *70*, 367−372. (e) Welborn, V. V.; Ruiz Pestana, L.; Head-Gordon, T. Computational Optimization of Electric Fields for Better Catalysis Design. *Nat. Catal.* **2018**, *1*, 649−655. (f) Acosta-Silva, C.; Bertran, J.; Branchadell, V.; Oliva, A. Kemp Elimination Reaction Catalyzed by Electric Fields. *ChemPhysChem* **2020**, *21*, 295−306. (g) Stuyver, T.; Shaik, S. Resolving Entangled Reactivity Modes through External Electric Fields and Substitution: Application to E_2/S_N2 Reactions. *J. Org. Chem.* **2021**, *86*, 9030−9039.

(6) Hill, N. S.; Coote, M. L. Internal Oriented Electric Fields as a Strategy for Selectively Modifying Photochemical Reactivity. *J. Am. Chem. Soc.* **2018**, *140*, 17800−17804.

(7) Jaroš, A.; Bonab, E. F.; Straka, M.; Foroutan-Nejad, C. Fullerene-Based Switching Molecular Diodes Controlled by Oriented External Electric Fields. *J. Am. Chem. Soc.* **2019**, *141*, 19644−19654.

(8) Kirshenboim, O.; Frenklah, A.; Kozuch, S. Switch Chemistry at Cryogenic Conditions: Quantum Tunnelling under Electric Fields. *Chem. Sci.* **2021**, *12*, 3179−3187.
(9) (a) Lei, Y. K.; Zhang, J.; Zhang, Z.; Gao, Y. Q. Dynamic Electric Field Complicates Chemical Reactions in Solutions. *J. Phys. Chem. Lett.* **2019**, *10*, 2991−2997. (b) Mattioli, E. J.; Bottoni, A.; Zerbetto, F.; Calvaresi, M. Oriented External Electric Fields Affect Rate and Stereoselectivity of Electrocyclic Reactions. *J. Phys. Chem. C* **2019**, *123*, 26370−26378. (c) Shi, M. W.; Thomas, S. P.; Hathwar, V. R.; Edwards, A. J.; Piltz, R. O.; Jayatilaka, D.; Koutsantonis, G. A.; Overgaard, J.; Nishibori, E.; Iversen, B. B.; Spackman, M. A. Measurement of Electric Fields Experienced by Urea Guest Molecules in the 18-Crown-6/Urea (1:5) Host−Guest Complex: An Experimental Reference Point for Electric-Field-Assisted Catalysis. *J. Am. Chem. Soc.* **2019**, *141*, 3965−3976. (d) Smolinsky, E. Z. B.; Neubauer, A.; Kumar, A.; Yochelis, S.; Capua, E.; Carmieli, R.; Paltiel, Y.; Naaman, R.; Michaeli, K. Electric Field-Controlled Magnetization in GaAs/AlGaAs Heterostructures−Chiral Organic Molecules Hybrids. *J. Phys. Chem. Lett.* **2019**, *10*, 1139−1145. (e) Wang, C.; Danovich, D.; Chen, H.; Shaik, S. Oriented External Electric Fields: Tweezers and Catalysts for Reactivity in Halogen-Bond Complexes. *J. Am. Chem. Soc.* **2019**, *141*, 7122−7136. (f) Yeh, C.-H.; Pham, T. M. L.; Nachimuthu, S.; Jiang, J.-C. Effect of External Electric Field on Methane Conversion on IrO_2(110) Surface: A Density Functional Theory Study. *ACS Catal.* **2019**, *9*, 8230−8242. (g) Zhang, M.-X.; Xu, H.-L. A Greener Catalyst for Hydroboration of Imines—External Electric Field Modify the Reaction Mechanism. *J. Comput. Chem.* **2019**, *40*, 1772−1779. (h) He, C. Q.; Lam, C. C.; Yu, P.; Song, Z.; Chen, M.; Lam, Y.-h.; Chen, S.; Houk, K. N. Catalytic Effects of Ammonium and Sulfonium Salts and External Electric Fields on Aza-Diels−Alder Reactions. *J. Org. Chem.* **2020**, *85*, 2618−2625. (i) Wang, W.-W.; Shang, F.-L.; Zhao, X. Curved Carbon Skeleton in Oriented External Electric Fields: Modulated Curvature, Directional Bowl Inversion, and Face-Selective Cycloadditions of Corannulene. *Org. Lett.* **2020**, *22*, 4786−4791. (j) Zhang, R.; Warren, J. J. Controlling the Oxygen Reduction Selectivity of Asymmetric Cobalt Porphyrins by Using Local Electrostatic Interactions. *J. Am. Chem. Soc.* **2020**, *142*, 13426−13434. (k) Gheorghiu, A.; Coveney, P. V.; Arabi, A. A. The Influence of External Electric Fields on Proton Transfer Tautomerism in the Guanine−Cytosine Base Pair. *Phys. Chem. Chem. Phys.* **2021**, *23*, 6252−6265. (l) Hennefarth, M. R.; Alexandrova, A. N. Heterogeneous Intramolecular Electric Field as a Descriptor of Diels−Alder Reactivity. *J. Phys. Chem. A* **2021**, *125*, 1289−1298. (m) Martin, D. J.; Mayer, J. M. Oriented Electrostatic Effects on O_2 and CO_2 Reduction by a Polycationic Iron Porphyrin. *J. Am. Chem. Soc.* **2021**, *143*, 11423−11434. (n) Mejía, L.; Garay-Ruiz, D.; Franco, I. Diels−Alder Reaction in a Molecular Junction. *J. Phys. Chem. C* **2021**, *125*, 14599−14606. (o) Wang, W.-W.; Shang, F.-L.; Zhao, X. Switchable (2 + 2) and (4 + 2) Cycloadditions on Boron Nitride Nanotubes under Oriented External Electric Fields: A Mechanistic Study. *J. Org. Chem.* **2021**, *86*, 3785−3791.
(10) (a) Ciampi, S.; Darwish, N.; Aitken, H. M.; Díez-Pérez, I.; Coote, M. L. Harnessing Electrostatic Catalysis in Single Molecule, Electrochemical and Chemical Systems: a Rapidly Growing Experimental Tool Box. *Chem. Soc. Rev.* **2018**, *47*, 5146−5164. (b) Simpson, G. J.; García-López, V.; Daniel Boese, A.; Tour, J. M.; Grill, L. How to control single-molecule rotation. *Nat. Commun.* **2019**, *10*, No. 4631.
(11) Bandrauk, A. D.; Sedik, E.-W. S.; Matta, C. F. Effect of Absolute Laser Phase on Reaction Paths in Laser-Induced Chemical Reactions. *J. Chem. Phys.* **2004**, *121*, 7764−7775.
(12) Climent, C.; Galego, J.; Garcia-Vidal, F. J.; Feist, J. Plasmonic Nanocavities Enable Self-Induced Electrostatic Catalysis. *Angew. Chem., Int. Ed.* **2019**, *58*, 8698−8702.
(13) (a) Li, A.; Zi, Y.; Guo, H.; Wang, Z. L.; Fernández, F. M. Triboelectric Nanogenerators for Sensitive Nano-Coulomb Molecular Mass Spectrometry. *Nat. Nanotechnol.* **2017**, *12*, 481−487. (b) Xia, H.; Wang, Z. Piezoelectricity Drives Organic Synthesis. *Science* **2019**, *366*, 1451−1452. (c) Zhang, J.; Ciampi, S. Shape and Charge:
(14) Grahame, D. C. The Electrical Double Layer and the Theory of Electrocapillarity. *Chem. Rev.* **1947**, *41*, 441−501.
(15) Heo, J.; Ahn, H.; Won, J.; Son, J. G.; Shon, H. K.; Lee, T. G.; Han, S. W.; Baik, M. H. Electro-inductive effect: Electrodes as functional groups with tunable electronic properties. *Science* **2020**, *370*, 214−219.
(16) Patrow, J. G.; Sorenson, S. A.; Dawlaty, J. M. Direct Spectroscopic Measurement of Interfacial Electric Fields near an Electrode under Polarizing or Current-Carrying Conditions. *J. Phys. Chem. C* **2017**, *121*, 11585−11592.
(17) (a) Ge, A.; Videla, P. E.; Lee, G. L.; Rudshteyn, B.; Song, J.; Kubiak, C. P.; Batista, V. S.; Lian, T. Interfacial Structure and Electric Field Probed by in Situ Electrochemical Vibrational Stark Effect Spectroscopy and Computational Modeling. *J. Phys. Chem. C* **2017**, *121*, 18674−18682. (b) Clark, M. L.; Ge, A.; Videla, P. E.; Rudshteyn, B.; Miller, C. J.; Song, J.; Batista, V. S.; Lian, T.; Kubiak, C. P. CO_2 Reduction Catalysts on Gold Electrode Surfaces Influenced by Large Electric Fields. *J. Am. Chem. Soc.* **2018**, *140*, 17643−17655. (c) Ge, A.; Rudshteyn, B.; Videla, P. E.; Miller, C. J.; Kubiak, C. P.; Batista, V. S.; Lian, T. Heterogenized Molecular Catalysts: Vibrational Sum-Frequency Spectroscopic, Electrochemical, and Theoretical Investigations. *Acc. Chem. Res.* **2019**, *52*, 1289−1300.
(18) (a) Fried, S. D.; Boxer, S. G. Electric Fields and Enzyme Catalysis. *Annu. Rev. Biochem.* **2017**, *86*, 387−415. (b) Vaissier Welborn, V.; Head-Gordon, T. Computational Design of Synthetic Enzymes. *Chem. Rev.* **2019**, *119*, 6613−6630. (c) Bím, D.; Alexandrova, A. N. Electrostatic Regulation of Blue Copper Sites. *Chem. Sci.* **2021**, *12*, 11406−11413.
(19) (a) Shaik, S.; de Visser, S. P.; Kumar, D. External Electric Field Will Control the Selectivity of Enzymatic-Like Bond Activations. *J. Am. Chem. Soc.* **2004**, *126*, 11746−11749. (b) Schyman, P.; Lai, W.; Chen, H.; Wang, Y.; Shaik, S. The Directive of the Protein: How Does Cytochrome P450 Select the Mechanism of Dopamine Formation? *J. Am. Chem. Soc.* **2011**, *133*, 7977−7984. (c) Stuyver, T.; Ramanan, R.; Mallick, D.; Shaik, S. Oriented (Local) Electric Fields Drive the Millionfold Enhancement of the H-Abstraction Catalysis Observed for Synthetic Metalloenzyme Analogues. *Angew. Chem., Int. Ed.* **2020**, *59*, 7915−7920. (d) Bím, D.; Alexandrova, A. N. Local Electric Fields As a Natural Switch of Heme-Iron Protein Reactivity. *ACS Catal.* **2021**, *11*, 6534−6546. (e) Ramanan, R.; Waheed, S. O.; Schofield, C. J.; Christov, C. Z. What Is the Catalytic Mechanism of Enzymatic Histone N-Methyl Arginine Demethylation and Can It Be Influenced by an External Electric Field? *Chem.—Eur. J.* **2021**, *27*, 11827−11836.
(20) Li, W.-L.; Head-Gordon, T. Catalytic Principles from Natural Enzymes and Translational Design Strategies for Synthetic Catalysts. *ACS Cent. Sci.* **2021**, *7*, 72−80.
(21) Liu, C. T.; Layfield, J. P.; Stewart, R. J.; French, J. B.; Hanoian, P.; Asbury, J. B.; Hammes-Schiffer, S.; Benkovic, S. J. Probing the Electrostatics of Active Site Microenvironments along the Catalytic Cycle for Escherichia coli Dihydrofolate Reductase. *J. Am. Chem. Soc.* **2014**, *136*, 10349−10360.
(22) (a) Bhowmick, A.; Sharma, S. C.; Head-Gordon, T. The Importance of the Scaffold for de Novo Enzymes: A Case Study with Kemp Eliminase. *J. Am. Chem. Soc.* **2017**, *139*, 5793−5800. (b) Welborn, V. V.; Head-Gordon, T. Fluctuations of Electric Fields in the Active Site of the Enzyme Ketosteroid Isomerase. *J. Am. Chem. Soc.* **2019**, *141*, 12487−12492.
(23) Vaissier, V.; Sharma, S. C.; Schaettle, K.; Zhang, T.; Head-Gordon, T. Computational Optimization of Electric Fields for Improving Catalysis of a Designed Kemp Eliminase. *ACS Catal.* **2018**, *8*, 219−227.
(24) Stuyver, T.; Huang, J.; Mallick, D.; Danovich, D.; Shaik, S. TITAN: A Code for Modeling and Generating Electric Fields—Features and Applications to Enzymatic Reactivity. *J. Comput. Chem.* **2020**, *41*, 74−82.
(25) Shaik, S.; Danovich, D.; Dubey, K. D.; Stuyver, T. The Impact of Electric Fields on Chemical Structure and Reactivity. In *Effects of*

Electric Fields on Structure and Reactivity: New Horizons in Chemistry; Shaik, S.; Stuyver, T., Eds.; Royal Society of Chemistry: Cambridge, 2021; Chapter 2, pp 12−70.
(26) (a) Luis, J. M.; Duran, M.; Andrés, J. L. A Systematic and Feasible Method for Computing Nuclear Contributions to Electrical Properties of Polyatomic Molecules. *J. Chem. Phys.* **1997**, *107*, 1501−1512. (b) Kirtman, B.; Luis, J. M.; Bishop, D. M. Simple Finite Field Method for Calculation of Static and Dynamic Vibrational Hyperpolarizabilities: Curvature Contributions. *J. Chem. Phys.* **1998**, *108*, 10008−10012. (c) Luis, J. M.; Martí, J.; Duran, M.; Andrés, J. L.; Kirtman, B. Nuclear Relaxation Contribution to Static and Dynamic (Infinite Frequency Approximation) Nonlinear Optical Properties by means of Electrical Property Expansions: Application to HF, CH_4, CF_4, and SF6. *J. Chem. Phys.* **1998**, *108*, 4123−4130.
(27) (a) Torrent-Sucarrat, M.; Solà, M.; Duran, M.; Luis, J. M.; Kirtman, B. Initial Convergence of the Perturbation Series Expansion for Vibrational Nonlinear Optical Properties. *J. Chem. Phys.* **2002**, *116*, 5363−5373. (b) Torrent-Sucarrat, M.; Solà, M.; Duran, M.; Luis, J. M.; Kirtman, B. Basis Set and Electron Correlation Effects on ab Initio Electronic and Vibrational Nonlinear Optical Properties of Conjugated Organic Molecules. *J. Chem. Phys.* **2003**, *118*, 711−718. (c) Torrent-Sucarrat, M.; Solà, M.; Duran, M.; Luis, J. M.; Kirtman, B. Basis Set and Electron Correlation Effects on Initial Convergence for Vibrational Nonlinear Optical Properties of Conjugated Organic Molecules. *J. Chem. Phys.* **2004**, *120*, 6346−6355. (d) Torrent-Sucarrat, M.; Luis, J. M.; Kirtman, B. Variational Calculation of Vibrational Linear and Nonlinear Optical Properties. *J. Chem. Phys.* **2005**, *122*, No. 204108.
(28) Frisch, M. J.; Trucks, G. W.; Schlegel, H. B.; Scuseria, G. E.; Robb, M. A.; Cheeseman, J. R.; Scalmani, G.; Barone, V.; Petersson, G. A.; Nakatsuji, H.; Li, X.; Caricato, M.; Marenich, A. V.; Bloino, J.; Janesko, B. G.; Gomperts, R.; Mennucci, B.; Hratchian, H. P.; Ortiz, J. V.; Izmaylov, A. F.; Sonnenberg, J. L.; Williams; Ding, F.; Lipparini, F.; Egidi, F.; Goings, J.; Peng, B.; Petrone, A.; Henderson, T.; Ranasinghe, D.; Zakrzewski, V. G.; Gao, J.; Rega, N.; Zheng, G.; Liang, W.; Hada, M.; Ehara, M.; Toyota, K.; Fukuda, R.; Hasegawa, J.; Ishida, M.; Nakajima, T.; Honda, Y.; Kitao, O.; Nakai, H.; Vreven, T.; Throssell, K.; Montgomery, J. A., Jr.; Peralta, J. E.; Ogliaro, F.; Bearpark, M. J.; Heyd, J. J.; Brothers, E. N.; Kudin, K. N.; Staroverov, V. N.; Keith, T. A.; Kobayashi, R.; Normand, J.; Raghavachari, K.; Rendell, A. P.; Burant, J. C.; Iyengar, S. S.; Tomasi, J.; Cossi, M.; Millam, J. M.; Klene, M.; Adamo, C.; Cammi, R.; Ochterski, J. W.; Martin, R. L.; Morokuma, K.; Farkas, O.; Foresman, J. B.; Fox, D. J. *Gaussian 16*, revision C.01; Gaussian, Inc.: Wallingford, CT, 2016.
(29) (a) Vosko, S. H.; Wilk, L.; Nusair, M. Accurate Spin-Dependent Electron Liquid Correlation Energies for Local Spin Density Calculations: a Critical Analysis. *Can. J. Phys.* **1980**, *58*, 1200−1211. (b) Lee, C.; Yang, W.; Parr, R. G. Development of the Colle-Salvetti Correlation-Energy Formula into a Functional of the Electron Density. *Phys. Rev. B* **1988**, *37*, 785−789. (c) Becke, A. D. Density-Functional Thermochemistry. III. The Role of Exact Exchange. *J. Chem. Phys.* **1993**, *98*, 5648−5652.
(30) Ditchfield, R.; Hehre, W. J.; Pople, J. A. Self-Consistent Molecular-Orbital Methods. IX. An Extended Gaussian-Type Basis for Molecular-Orbital Studies of Organic Molecules. *J. Chem. Phys.* **1971**, *54*, 724−728.
(31) Grimme, S.; Antony, J.; Ehrlich, S.; Krieg, H. A Consistent and Accurate ab Initio Parametrization of Density Functional Dispersion Correction (DFT-D) for the 94 Elements H-Pu. *J. Chem. Phys.* **2010**, *132*, No. 154104.
(32) (a) Johnson, E. R.; Becke, A. D. A Post-Hartree-Fock Model of Intermolecular Interactions: Inclusion of Higher-Order Corrections. *J. Chem. Phys.* **2006**, *124*, No. 174104. (b) Grimme, S.; Ehrlich, S.; Goerigk, L. Effect of the Damping Function in Dispersion Corrected Density Functional Theory. *J. Comput. Chem.* **2011**, *32*, 1456−1465.
(33) (a) Perdew, J. P. Density-Functional Approximation for the Correlation Energy of the Inhomogeneous Electron Gas. *Phys. Rev. B* **1986**, *33*, 8822−8824. (b) Becke, A. D. Density-Functional Exchange-Energy Approximation with Correct Asymptotic Behavior. *Phys. Rev. A* **1988**, *38*, 3098−3100.
(34) Murgida, D. H.; Hildebrandt, P. Electron-Transfer Processes of Cytochrome c at Interfaces. New Insights by Surface-Enhanced Resonance Raman Spectroscopy. *Acc. Chem. Res.* **2004**, *37*, 854−861.
(35) Dubey, K. D.; Stuyver, T.; Kalita, S.; Shaik, S. Solvent Organization and Rate Regulation of a Menshutkin Reaction by Oriented External Electric Fields are Revealed by Combined MD and QM/MM Calculations. *J. Am. Chem. Soc.* **2020**, *142*, 9955−9965.
(36) Fernández, S.; Franco, F.; Casadevall, C.; Martin-Diaconescu, V.; Luis, J. M.; Lloret-Fillol, J. A Unified Electro- and Photocatalytic CO2 to CO Reduction Mechanism with Aminopyridine Cobalt Complexes. *J. Am. Chem. Soc.* **2020**, *142*, 120−133.
(37) Hoffmann, R.; Schleyer, P. v. R.; Schaefer, H. F., III Predicting Molecules—More Realism, Please! *Angew. Chem., Int. Ed.* **2008**, *47*, 7164−7167.
(38) (a) Huisgen, R. 1,3-Dipolar Cycloadditions. Past and Future. *Angew. Chem., Int. Ed.* **1963**, *2*, 565−598. (b) Huisgen, R. *1,3-Dipolar Cycloaddition Chemistry*; John Wiley & Sons, Inc.: New York, 1984; Vol. *1*, pp 1−176. (c) Breugst, M.; Reissig, H.-U. The Huisgen Reaction: Milestones of the 1,3-Dipolar Cycloaddition. *Angew. Chem., Int. Ed.* **2020**, *59*, 12293−12307.
(39) (a) de Cózar, A.; Cossío, F. P. Stereocontrolled (3+2) Cycloadditions between Azomethine Ylides and Dipolarophiles: a Fruitful Interplay between Theory and Experiment. *Phys. Chem. Chem. Phys.* **2011**, *13*, 10858−10868. (b) Arrastia, I.; Arrieta, A.; Cossío, F. P. Application of 1,3-Dipolar Reactions between Azomethine Ylides and Alkenes to the Synthesis of Catalysts and Biologically Active Compounds. *Eur. J. Org. Chem.* **2018**, *2018*, 5889−5904.
(40) Arrieta, A.; Otaegui, D.; Zubia, A.; Cossío, F. P.; Díaz-Ortiz, A.; de la Hoz, A.; Herrero, M. A.; Prieto, P.; Foces-Foces, C.; Pizarro, J. L.; Arriortua, M. I. Solvent-Free Thermal and Microwave-Assisted [3 + 2] Cycloadditions between Stabilized Azomethine Ylides and Nitrostyrenes. An Experimental and Theoretical Study. *J. Org. Chem.* **2007**, *72*, 4313−4322.
(41) Rivilla, I.; Odriozola-Gimeno, M.; Aires, A.; Gimeno, A.; Jiménez-Barbero, J.; Torrent-Sucarrat, M.; Cortajarena, A. L.; Cossío, F. P. Discovering Biomolecules with Huisgenase Activity: Designed Repeat Proteins as Biocatalysts for (3 + 2) Cycloadditions. *J. Am. Chem. Soc.* **2020**, *142*, 762−776.
(42) Diels, O.; Alder, K. Synthesen in der Hydroaromatischen Reihe. *Justus Liebigs Ann. Chem.* **1928**, *460*, 98−122.
(43) Fringuelli, F. T. A. *The Diels−Alder Reaction: Selected Practical Methods.*; John Wiley & Sons: Chichester, England, 2002.
(44) (a) Rogers, F. E.; Quan, S. W. Thermochemistry of the Diels-Alder Reaction. III. Heat of addition of Cyclopentadiene to Maleic Anhydride. *J. Phys. Chem. B.* **1973**, *77*, 828−831. (b) Breslauer, K. J.; Kabakoff, D. S. Enthalpy of the Diels-Alder Reaction of Cyclopentadiene and Maleic Anhydride. *J. Org. Chem.* **1974**, *39*, 721−722.
(45) Yu, S.; Vermeeren, P.; Hamlin, T. A.; Bickelhaupt, F. M. How Oriented External Electric Fields Modulate Reactivity. *Chem.—Eur. J.* **2021**, *27*, 5683−5693.
(46) Wannere, C. S.; Paul, A.; Herges, R.; Houk, K. N.; Schaefer, H. F., III; Schleyer, P. v. R. The Existence of Secondary Orbital Interactions. *J. Comput. Chem.* **2007**, *28*, 344−361.
(47) (a) Arabi, A. A.; Matta, C. F. Effects of external electric fields on double proton transfer kinetics in the formic acid dimer. *Phys. Chem. Chem. Phys.* **2011**, *13*, 13738−13748. (b) Sowlati-Hashjin, S.; Matta, C. F. The chemical bond in external electric fields: Energies, geometries, and vibrational Stark shifts of diatomic molecules. *J. Chem. Phys.* **2013**, *139*, No. 144101. (c) Sowlati-Hashjin, S.; Karttunen, M.; Matta, C. F. Manipulation of Diatomic Molecules with Oriented External Electric Fields: Linear Correlations in Atomic Properties Lead to Nonlinear Molecular Responses. *J. Phys. Chem. A* **2020**, *124*, 4720−4731.
(48) (a) Bell, R. P. The Theory of Reactions Involving Proton Transfers. *Proc. R. Soc. London, Ser. A* **1936**, *154*, 414−429. (b) Evans, M. G.; Polanyi, M. On the Introduction of Thermodynamic Variables into Reaction Kinetics. *Trans. Faraday Soc.* **1937**, *33*, 448−452.

(49) (a) Osuna, S.; Morera, J.; Cases, M.; Morokuma, K.; Solà, M. Diels−Alder Reaction between Cyclopentadiene and C_{60}: An Analysis of the Performance of the ONIOM Method for the Study of Chemical Reactivity in Fullerenes and Nanotubes. *J. Phys. Chem. A* **2009**, *113*, 9721−9726. (b) Osuna, S.; Swart, M.; Solà, M. Dispersion Corrections Essential for the Study of Chemical Reactivity in Fullerenes. *J. Phys. Chem. A* **2011**, *115*, 3491−3496. (c) Fernández, I.; Solà, M.; Bickelhaupt, F. M. Why Do Cycloaddition Reactions Involving C60 Prefer [6,6] over [5,6] Bonds? *Chem.—Eur. J.* **2013**, *19*, 7416−7422.

(50) Pang, L. S. K.; Wilson, M. A. Reactions of Fullerenes C_{60} and C_{70} with Cyclopentadiene. *J. Phys. Chem. C.* **1993**, *97*, 6761−6763.

(51) Garcia-Borràs, M.; Osuna, S.; Swart, M.; Luis, J. M.; Solà, M. Electrochemical Control of the Regioselectivity in the Exohedral Functionalization of C_{60}: the Role of Aromaticity. *Chem. Commun.* **2013**, *49*, 1220−1222.

(52) El Bakouri, O.; Garcia-Borràs, M.; Girón, R. M.; Filippone, S.; Martín, N.; Solà, M. On the Regioselectivity of the Diels−Alder Cycloaddition to C_{60} in High Spin States. *Phys. Chem. Chem. Phys.* **2018**, *20*, 11577−11585.